PCCP

Cite this: *Phys. Chem. Chem. Phys.*, 2011, **13**, 14750–14757

www.rsc.org/pccp

PAPER

He-atom scattering from MgO(100): calculating diffraction peak intensities with a semi *ab initio* potential

R. Martinez-Casado,*[a] G. Mallia,[a] D. Usvyat,[b] L. Maschio,[cd] S. Casassa,[cd] M. Schütz[b] and N. M. Harrison[ae]

Received 16th April 2011, Accepted 13th June 2011
DOI: 10.1039/c1cp21212e

An efficient model describing the He-atom scattering process is presented. The He–surface interaction potential is calculated from first principles by exploiting second-order Rayleigh–Schrödinger many-body perturbation theory and fitted by using a variety of pairwise interaction potentials. The attractive part of the fitted analytical form has been upscaled to compensate the underestimation of the well depth for this system in the perturbation theory description. The improved potential has been introduced in the close-coupling method to calculate the diffraction pattern. Quantitative agreement between the computed and observed binding energy and diffraction intensities for the He–MgO(100) system is achieved. It is expected that the utility of He scattering for probing dynamical processes at surfaces will be significantly enhanced by this quantitative description.

I. Introduction

An understanding of surface structure and dynamics underpins all of surface science, heterogeneous catalysis, much of nano-science, and the technologies based on them. In response to this need the number of studies on oxide surfaces has increased rapidly in recent years and progress has been summarised in a number of articles.[1–3] Despite very careful investigations and optimized methods, inherent problems remain: oxides are insulating materials, for which all methods using or producing electrons are frequently hampered by artifacts due to charging or due to damage produced by impinging electrons. In some cases, the use of very low electron currents, nowadays available in channel plate low-energy electron diffraction (LEED) systems, reduces these artifacts.[4] In other cases, for example ZnO or TiO_2, a conduction mechanism *via* defects facilitates the use of scanning tunnelling microscopy (STM), LEED and other well-developed standard techniques. Except for the cleavage faces of the rocksalt-type oxides, MgO, NiO and CoO,[5–8] on most oxide surfaces usually a comparatively large defect density is present, which decreases the reliability of methods which cannot distinguish between a signal from well-ordered parts of the surface and a signal from defective parts, like photoelectron spectroscopy (XPS) or thermal desorption spectroscopy (TDS). He-atom scattering is a technique which uses neutral particles of sub-thermal energy (100 meV) and, therefore, is not complicated by charging and damaging effects and is sensitive only to the outermost layer; see ref. 9 and references therein.

Since the first diffraction He-atom scattering (HAS) experiment in 1930 by Estermann and Stern[10] on the (100) crystal face of lithium fluoride, the scattering of He atoms from surfaces has been widely used in solid state physics/chemistry to study and characterize the surface atomic structure. However, it was not until a third generation of nozzle beam sources was developed, around 1980, that studies of surface phonons using helium atom scattering were possible. These nozzle beam sources were capable of producing helium atom beams with an energy resolution of less than 1 meV, allowing explicit resolution of the very small energy changes resulting from the inelastic collision of a helium atom with the vibrational modes of a solid surface. This extended HAS to the study of surface lattice dynamics. The first measurement of such a surface phonon dispersion curve was reported in 1981,[11] leading to a renewed interest in helium atom scattering applications, particularly for the study of surface dynamics. The use of He-scattering has an important limitation, namely, the difficulties involved in the quantitative interpretation of the experimental diffraction patterns due to the lack of a detailed understanding of the scattering potential and process.

The quantitative analysis and correct interpretation of He-atom experiments basically consists of two steps: determining the He–surface interaction potential and then using dynamical quantum mechanical methods to compute the diffraction intensities. Empirical potentials modelling the He–surface interaction can be inadequate as they may miss the essential physics; these

[a] *Thomas Young Centre, Department of Chemistry, Imperial College London, South Kensington, London SW7 2AZ, UK. E-mail: r.martinezcasado@imperial.ac.uk*
[b] *Univ Regensburg, Inst Phys & Theoret Chem, D-93040 Regensburg, Germany*
[c] *Univ Turin, Dipartimento Chim, IFM, I-10125 Turin, Italy*
[d] *Univ Turin, Ctr Excellence NIS, I-10125 Turin, Italy*
[e] *Daresbury Laboratory, Daresbury, Warrington, WA4 4AD, UK*

potentials can only be used with confidence in a few well understood systems, and therefore undermine both the generality and accuracy of the structural determination.[12,13] Removing this limitation would have significant consequences for the general applicability of the technique. A first-principle He–surface interaction potential is difficult to obtain, because computer codes based on density functional theory (DFT) or Hartree–Fock (HF) include a poor treatment of long range weak intermolecular interactions. It has been shown[14] that a full *ab initio* potential can be obtained by using second-order Rayleigh–Schrödinger perturbation theory in the Møller–Plesset partitioning (MP2), as implemented in the computer code CRYSCOR,[15,16] for the evaluation of post-HF effects in the properties of periodic, non-conducting systems.

This study is aimed at developing an efficient model of the He–surface interaction to provide a convenient and reliable description of the He-atom scattering process. Firstly, the quantum-mechanical calculation of the He–surface interaction is based on exploiting second-order Møller–Plesset perturbation theory to approximate the correlation energy contribution to the London dispersion interaction. Secondly, a pairwise potential has been adopted to represent the He–surface interaction in order to separate repulsive and attractive contributions to the interaction and to provide a convenient representation for efficient close-coupling (CC) calculations.[17–20] Finally, an upscaling factor can be introduced for the attractive part of the fitted potential that allows one to correct its underestimation in the low-order perturbative approach. The objective of this paper is to present the results of the fitting of the He–surface interaction with the pairwise potential and the quantitative comparison of diffraction peaks with the observed diffraction intensities.

The paper is organised as follows: Sec. II contains computational details. In Sec. III the results for the He–MgO(100) interaction potential fitting and the diffraction spectra are presented and discussed. The main conclusions of this study are summarised in Sec. IV and the analytical form of the pairwise potential are documented in Appendix A.

II. Methodology and computational details

In order to study the He-atom scattering process the time-independent Schrödinger equation has to be solved for all the nuclei and electrons involved. The slow timescales associated with nuclear motions, in comparison with the electron dynamics, often allow us to assume the nuclear background to be static. This is the so-called Born–Oppenheimer (BO) approximation, which consists in two steps. In the first step the electronic Schrödinger equation is solved, yielding the electronic wave function with the nuclei fixed at particular configurations. This electronic computation must be repeated for many different nuclear configurations to produce a potential energy surface or, as in the current case, analytic representation of the He–MgO interaction potential. In the second step of the BO approximation, this potential is included in a Schrödinger equation containing only the nuclei, which must be solved numerically to obtain the quantum dynamics. In what follows, these two steps are explained in more detail.

A. Calculation of the He–MgO interaction potential

The interaction between He and the surface has been explored by considering a set of configurations, where the distance between the atom and the outermost layer has been varied in order to obtain the He–MgO interaction potential ($V(\mathbf{R}, z)$, where $\mathbf{R} = (x, y)$ and z is the direction perpendicular to the surface). The MgO(100) surface is approximated as a rigid 2D periodic 3 atomic layer sheet cut from the bulk structure at the experimental lattice constant ($a = 4.211$ Å).[21] The description of the He–MgO interaction is analysed by computing the binding energy of an isolated He atom and the clean surface.[22] Adsorption of the He atom has been considered over all the MgO unit cell (200 points) with a separation in z between the He atom and the outermost layer in the range: 3 Å–7 Å. A 2×2 supercell of the primitive surface unit cell is found to be sufficient to reduce the He–He lateral interactions to negligible values. All calculations have been performed using the CRYSTAL09[23,24] and CRYSCOR09[15,16] software packages, both based on the expansion of the crystalline orbitals as a linear combination of a local basis set (BS) consisting of atom centred Gaussian orbitals (see ref. 14 for details).

B. Dynamics: the close-coupling (CC) method

The He-surface dynamics has been described as the elastic scattering of structureless, non-penetrating particles off a statically corrugated periodic solid surface. A detailed formalism of the close-coupling method can be found *e.g.* in ref. 17; here we briefly outline the main principles. The momentum of the He particles is defined as $\mathbf{k} \equiv (\mathbf{K}, k_z)$, where $\mathbf{K}$ is the projection of the momentum vector parallel to the plane of surface and k_z is the perpendicular component. By the Bragg or diffraction condition the parallel momentum conservation is given by $\Delta\mathbf{K} = \mathbf{K}_f - \mathbf{K}_i = \mathbf{G}$, where $\mathbf{K}_f$ and $\mathbf{K}_i$ are the final and initial parallel momentum vectors, respectively, and $\mathbf{G}$ is a vector of the 2D reciprocal lattice associated with the periodic surface structure. The CC equations are derived[25] from the time-independent Schrödinger equation for a particle of mass μ (in HAS, μ is the He atom mass) and momentum vector $\mathbf{k}_i$ incident on a potential $V(\mathbf{r})$

$$\left[\nabla^2 + k_i^2 - \frac{2\mu}{\hbar^2} V(\mathbf{r})\right] \Psi(\mathbf{r}) = 0 \qquad (1)$$

(in units where $\hbar^2/2\mu = 1$). Because of the surface periodicity, the potential $V(\mathbf{r})$ can be expressed as a Fourier series:

$$V(\mathbf{R}, z) = V_0(z) + \sum_{\mathbf{G} \neq 0} V_{\mathbf{G}}(z) e^{i\mathbf{G}\cdot\mathbf{R}} \qquad (2)$$

and the wave function can be also expanded as follows:[25]

$$\Psi(\mathbf{r}) = \sum_{\mathbf{G}} \psi_{\mathbf{G}}(z) e^{i(\mathbf{K}+\mathbf{G})\cdot\mathbf{R}} \qquad (3)$$

$V_{\mathbf{G}}(z)$ and $\Psi_{\mathbf{G}}(z)$ are the coefficients of a Fourier expansion of the potential and the wave functions, $V_0(z)$ is the laterally and thermally averaged interaction potential. After integrating

over the area of a single surface unit cell, the CC equations take the form:

$$\left(\frac{\mathrm{d}^2}{\mathrm{d}z^2} + \mathbf{k}^2_{\mathbf{G},z} - V_0(z)\right)\Psi_{\mathbf{G}}(z) = \sum_{\mathbf{G}'\neq\mathbf{G}} V_{\mathbf{G}-\mathbf{G}'}(z)\Psi_{\mathbf{G}'}(z) \quad (4)$$

where

$$\mathbf{k}^2_{\mathbf{G},z} = \mathbf{k}^2_{\mathrm{i}} - (\mathbf{K}_{\mathrm{i}} + \mathbf{G})^2 \quad (5)$$

gives the square of the momentum component oriented along the z-direction, sometimes called 'z-component kinetic energy' of the **G**-diffracted wave or **G**-channel. In the CC formalism two different types of diffraction channels are distinguished, depending on the sign of the z-component kinetic energy $\mathbf{k}^2_{\mathbf{G},z}$ in eqn (5): if $\mathbf{k}^2_{\mathbf{G},z}$ is positive, one has *open* or energetically accessible channels, and if negative, the channels are *closed* or energetically forbidden.

The close-coupling equations (4) are solved numerically by using the Fox-Goodwin algorithm[26] and subject to the usual boundary conditions,[25]

$$\psi_{\mathbf{G}}(z) \underset{z\to 0}{\longrightarrow} 0$$

$$\psi_{\mathbf{G}}(z) \underset{z\to\infty}{\longrightarrow} \begin{cases} k_z^{-1/2}\exp(-ik_z z)\delta_{\mathbf{G},0} + k_{\mathbf{G}z}^{-1/2} S_{\mathbf{G}} \exp(ik_{\mathbf{G}z} z) & \text{for open channels,} \\ \kappa_{\mathbf{G}z}^{1/2} S_{\mathbf{G}} \exp(-\kappa_{\mathbf{G}z} z) & \text{for closed channels.} \end{cases} \quad (6)$$

where $\kappa_{\mathbf{G}z} = (-k^2_{\mathbf{G}z})^{1/2}$. The amplitude $S_{\mathbf{G}}$ is related to the observable diffraction probability or intensity $I_{\mathbf{G}} = |S_{\mathbf{G}}|^2$, starting from the specular channel ($\mathbf{G} = 0$). In order to take into account the effect of the temperature, a Debye–Waller factor, $2W$, has been used,

$$2W = \frac{3\hbar^2 T_{\mathrm{S}}(k_{iz} + k_{fz})^2}{M k_{\mathrm{B}} \Theta_{\mathrm{D}}^2} \quad (7)$$

with Θ_{D} the Debye temperature, M the mass of a surface atom, and k_{B} the Boltzmann constant. The Beeby correction[27] has been also included to take into account the aceleration due to the attractive part of the potential, where the initial and final wave vectors have been replaced by:

$$k_z = \sqrt{k_z^2 + \frac{2\mu D}{\hbar^2}}, \quad (8)$$

where D is the well depth and k_z corresponds to k_{iz} or k_{fz}, respectively. The observed intensity can then be compared to $I^T_{\mathbf{G}}$,

$$I^T_{\mathbf{G}} = I^0_{\mathbf{G}} \exp(-2W), \quad (9)$$

where $I^T_{\mathbf{G}}$ and $I^0_{\mathbf{G}}$ are the intensities at a T and zero surface temperature, respectively.

III. Results

This section is divided in two parts. In the first, the fitting of the He–MgO interaction potential to different pairwise potential forms is analysed and the best fit model identified. In the second, the diffraction pattern computed for the best fit model is presented and compared with the measured He diffraction intensities along the [100] direction of the MgO(100) surface.

A. Fitting

The calculated *ab initio* potential has been fitted, by minimising the sum of squares using the program GULP,[28] to different pairwise potentials (whose analytical form and the corresponding parameters are described in detail in Appendix A). The sum of squares, which is a measure of the discrepancy between the data and an the model potential, is defined as;

$$F = \frac{1}{N_{\mathrm{points}}} \sum_{i=1}^{N_{\mathrm{points}}} \left(f_i^{\mathrm{comp}} - f_i^{\mathrm{pot}}\right)^2, \quad (10)$$

where N_{points} is the number of computed *ab initio* energies, f_i^{comp} and f_i^{pot} are the computed and empirical potential values, respectively. The parameters for each potential have been obtained by following the procedure described below. Firstly, the fit has been performed considering only a O–He interaction as this is expected to play the most important role in the description of the He-surface potential. Secondly, the Mg–He contribution has been included in the fitting calculation while fixing the previously obtained O–He parameters. Finally, both O–He and Mg–He parameters have been fitted simultaneously. This procedure has been adopted as in the full parameter space F has multiple local minima and the result of simple unconstrained optimisation is strongly influenced by starting conditions and subject to trapping in unphysical minima.

In Table 1 the fitted coefficients are reported for the pure O–He fit and the fully unconstrained fit for a variety of potential forms. In all the cases the contribution of the Mg–He interaction is negligible when compared to that of the O–He interaction as expected. It is interesting that for the Lennard-Jones, Morse and Buckingham potential forms the values of the O–He parameters are not affected significantly by the introduction of the Mg–He interaction while for both General forms ($m = 1$ and $m = 2$) the O–He short range potential is affected and becomes somewhat steeper when including the Mg–He interaction. F is improved when the He–Mg interaction is introduced in all cases but that of the Morse potential. At short range He–O repulsion dominates, the He–Mg contribution is typically negligible. At long range the attractive potential dominates and may contain both He–O and He–Mg contributions. The short range nature of the attractive component of the Morse potential precludes any substantial contribution from the He–Mg interaction. As a result, the parameters for the Morse potential, which are rounded to two significant digits in Table 1, look identical. The negligible contribution of the He–Mg interaction has been confirmed

Table 1 Fitting parameters for the considered pairwise potential. For each form the first line refers to the fitting taking into account only the He–O interaction, the second data row includes also the contribution of He–Mg

	ε_{HeO}/meV	σ_{HeO}/Å		ε_{HeMg}/meV	σ_{HeMg}/Å		F/meV^2
Lennard-Jones	3.4×10^{-1}	4.4					0.50
	3.4×10^{-1}	4.3		5.8×10^{-2}	4.4		0.29
	D_{HeO}/meV	a_{HeO}/Å^{-2}	r_{HeO}/Å	D_{HeMg}/meV	a_{HeMg}/Å^{-2}	r_{HeMg}/Å	F/meV^2
Morse	6.0×10^{-1}	1.3	4.5				0.23
	6.0×10^{-1}	1.3	4.5	1.7×10^{-1}	1.6	9.5×10^{-1}	0.23
	A_{HeO}/meV Å^m	ρ_{HeO}/Å	C_{HeO}/meV Å^6	A_{HeMg}/meV Å^m	ρ_{HeMg}/Å	C_{HeMg}/meV Å^6	F/meV^2
Buckingham (General (m = 0))	1.5×10^5	3.5×10^{-1}	7.0×10^3				0.30
	1.4×10^5	3.5×10^{-1}	6.3×10^3	2.1	4.5×10^{-1}	7.0×10^{-1}	0.24
General (m = 1)	5.6×10^4	4.6×10^{-1}	7.9×10^3				0.67
	2.2×10^5	3.8×10^{-1}	6.1×10^3	2.1×10^{-1}	5.5×10^{-1}	5.8×10^1	0.19
General (m = 2)	1.7×10^5	4.6×10^{-1}	6.8×10^3				0.28
	3.8×10^5	4.1×10^{-1}	5.9×10^3	2.7	4.4×10^{-1}	1.8×10^1	0.17

as well in a recent paper where a pairwise additive model has been used to describe the He–MgO interaction.[3] It is notable that the potential parameters are strongly correlated and so the determination of a unique fit for a given *ab initio* potential is extremely difficult to achieve.

The quality of the fit is assessed by comparing F of Table 1. All the studied potentials provide a similar value for F (0.17–0.29 meV^2). The best fit has been obtained for the General potential form (m = 2) followed in order of goodness of fit by the General (m = 1), Morse, Buckingham and Lennard-Jones forms. From Fig. 1 (and Fig. 2, where the reference HF + MP2 potentials are given), it is seen that the Lennard-Jones potential is on average the best in the long range, but fails in the short range due to the physically incorrect form of the repulsive component. The Morse potential performs somewhat oppositely. The Buckingham and General potentials demonstrate similar error patterns, with the General (m = 2) potential being on average the best. Therefore, the latter has been employed in Sec. III.B. The bound states of $V_0(z)$ for the modified potential, calculated by using the Numerov algorithm,[29] have been found to be: E_0 = −5.99 meV, E_1 = −3.09 meV, E_2 = −1.38 meV, E_3 = −0.51 meV and E_4 = −0.13 meV, which are in good agreement with the experimental values shown in the literatute.[6,30] The lowest level of −10.2 meV presented by

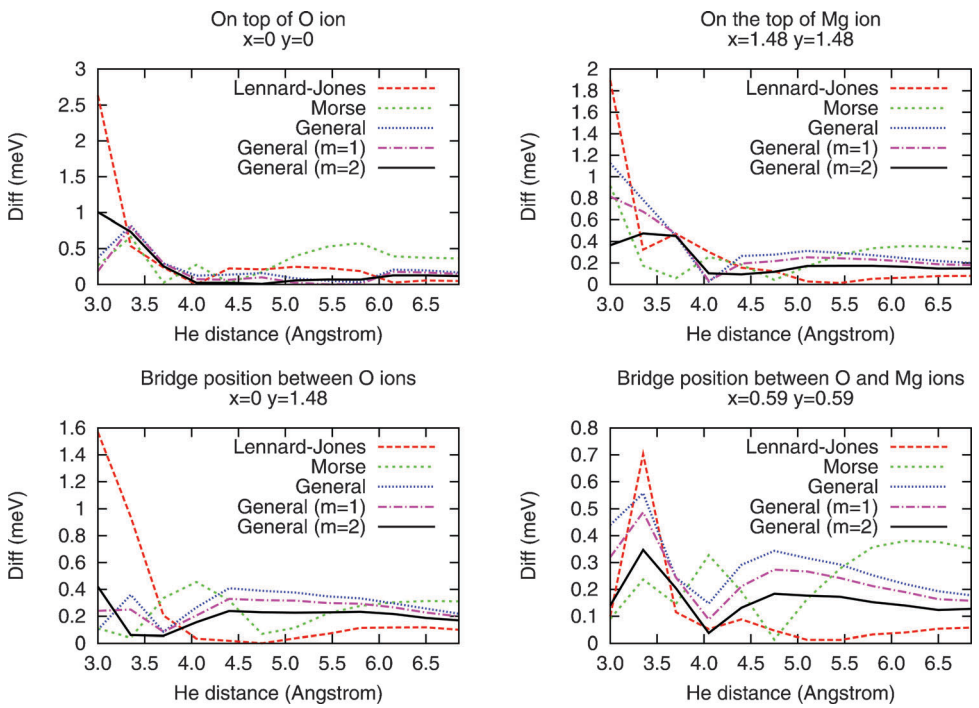

Fig. 1 Difference between the HF + MP2 data and the fitting with the following potential forms: Lennard-Jones (red long-dashed line), Morse (green short-dashed line), Buckingham (blue dotted line), General m = 1 (pink dashed-dotted line), and General m = 2 (black solid line). Four different positions of the He in the MgO unit cell have been considered: the x = 0.0, y = 0.0 position corresponds to the He on top of the O ion, the position x = 1.48, y = 1.48 to the He on top of the Mg ion and the positions x = 0.0, y = 1.48 and x = 0.59, y = 0.59 to bridge positions inside the unit cell (position coordinates in Å).

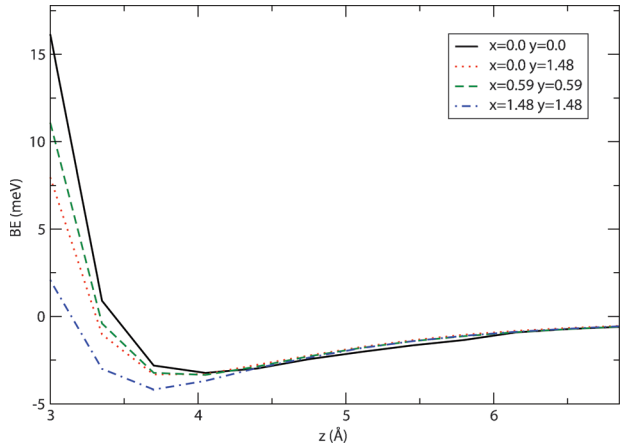

Fig. 2 HF + MP2 data for four different positions of the He in the MgO unit cell. The $x = 0.0$, $y = 0.0$ position (black solid line) corresponds to the He on top of the O ion, the position $x = 1.48$, $y = 1.48$ (dashed-dotted blue line) to the He on top of the Mg ion and the positions $x = 0.0$, $y = 1.48$ (dotted red line) and $x = 0.59$, $y = 0.59$ (dashed green line) to bridge positions inside the unit cell (position coordinates in Å).

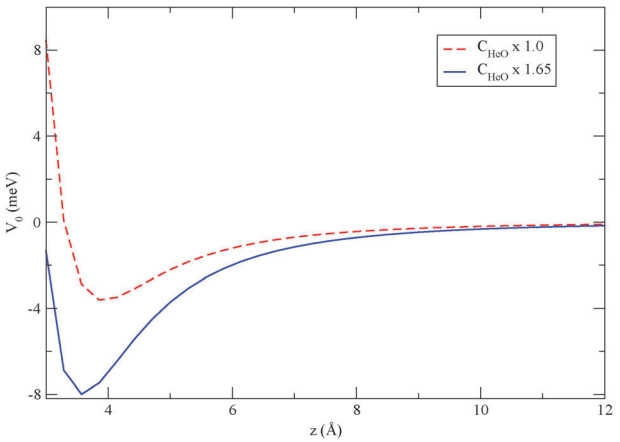

Fig. 3 Comparison of the averaged potential $V_0(z)$ for C_{HeO} = 5.8902 eV Å^6 (red dashed line) and $C_{HeO} \times 1.65$ (blue solid line). The x-axis corresponds to the perpendicular distance between the He atom and the first layer of the slab.

Benedek *et al.*[5,31] has not been found with our model potential. It has to be noticed that many other experimental measurements have failed in showing this level.[6,32,33] Having obtained a reliable fit for the interaction of He with the 3 atomic layers slab the interaction with the surface is computed by using the fit to extrapolate to infinite slab thickness. In practice a slab of 33 atomic layers produces an interaction within 1 meV of the infinite limit.

B. The computed diffraction pattern

The He–surface interaction potential, which is crucial for calculating the diffraction intensities, has been calculated previously within the HF + MP2 level of theory in ref. 14. Despite the correct qualitative description of the long range binding interaction, the computed well depth is significantly smaller than observed.[31,34] This behaviour has been documented for a number of intermolecular interactions and is generally assigned to an underestimation of the attractive dispersion interaction.[35,36] Indeed, the interaction between weakly polarizable systems (such as the He atoms and MgO slab in our case) is known to be noticeably underestimated by the MP2 method,[14,37,38] in contrast to highly polarizable ones, where MP2 notoriously overbinds. In order to compensate for this deficiency, the attractive part of the model potential can be upscaled to improve the results while still taking advantage of the correct shape of the curve obtained at the MP2 level. The upscaling factor for the C_{HeO} parameter (5.8902 eV Å^6) has been varied from 1.0 to 1.8. The values lower than 1.6 and higher than 1.7 yield a poor description of the diffraction peaks, when compared to the experimental data. Hence a value of 1.65 has been chosen for the upscaling factor, with which the diffraction intensities are in fact very well reproduced (*vide infra*). Interestingly, this fitted upscaling parameter 1.65 is quite close to the ratio between the CCSD(T) (aug-cc-pV(D/T)Z-extrapolated) and MP2 (aug-cc-pVTZ) well depths for a test cluster system He–$Mg_3Na_2O_4$, found to be 1.88.[14] However, this agreement should be taken with a grain of salt, since, firstly, the MP2 and CCSD(T) well depths correspond to slightly different He–Mg distances and, secondly, they implicitly involve the repulsive component of the interaction which was not upscaled in our case.

In Fig. 3 the planar averaged potential, $V_0(z)$, has been plotted for both the unmodified and modified potential for which the well depths are 3.4 meV (red line) and 8.0 meV (blue line), respectively. There is no firmly established observation of the well depth with values deduced from He-scattering spectra being in the range 7.5 meV–12.5 meV.[31,34,39] It has to be noticed that the well depth presented here is the same as the one obtained in ref. 39.

The expected long-range behaviour for a He atom interacting with a continuum dielectric or with the surface *via* a set of pairwise $1/r^6$ interactions is $1/z^3$ where z is the He–surface separation.[40] For both modified and unmodified potentials $V_0(z)$ reproduces this $1/z^3$ trend at long range. At the same time, as it is seen from Fig. 3, the upscaling of the attractive component has a distinct effect on the position of the repulsive wall, essential in the scattering process.

As it is not possible to take the infinite number of all (open and closed) channels into account, the calculation needs to be restricted to a finite number of **G** vectors. The number of **G** vectors has been determined by checking the convergence of the results with increasing number of channels included in the calculation. The number of channels needed for convergence usually depends on the incident energy E_i, but it is maintained in this case to 49 for all the considered spectra. The closed channels have to be taken into account in the calculation because the often observed phenomenon of bound state resonances[41] can significantly affect the diffraction probabilities due to the coupling of the open to the closed channels. The Fourier components to be included in eqn (2) have been obtained Fourier transforming both the modified and unmodified potentials over the unit cell. The CC calculation has shown that in order get a good description of the potential 9 terms need to be included in the Fourier series. These terms are the

corresponding to $G = 2\pi/a(n, m)$ with $(n, m) = (0, 0), (\pm1, 0), (0, \pm1), (\pm1, \pm1)$. This result proves that the corrugation function cannot be expressed in the simple form:

$$\xi(x, y) = h(\cos(2\pi x/a) + \cos(2\pi y/a)), \qquad (11)$$

as it has been accepted.[42] The corrugation function is commonly defined within simple models in order to determine if the chosen potential is able to describe the He–surface interaction. In our case, the corrugation depends explicitly on the He–surface distance. It is therefore not possible to define a realistic corrugation function. In previous works,[12,13] an effective corrugation function (depending on the incident energy) has been calculated by using DFT calculations. As it has been explained above DFT calculations are not suitable to determine the attractive part of the He–MgO interaction. Therefore these calculations has been restricted to the repulsive part of the interaction potential.

In Fig. 4, the He–surface diffraction peaks, calculated with the CC method, are shown for the unmodified (red stars) and modified (blue circles) potentials. Both the experimental peak intensity (black line) and the corresponding peak areas (black squares)[31] are shown, where the latter are a more reliable representation of the peak intensity than the peak height as the effects of diffraction peak broadening due to energy spread of the He beam are taken into account. The effects of temperature on the theoretical results have been included using a Debye–Waller with a Debye temperature of 495 K[43] determined by elastic neutron scattering at a surface temperature of 300 K.

There is reasonable agreement between the calculated diffraction intensities and those observed for all six He incident energies when the modified interaction potential is used; the agreement when the unmodified potential is used (or the raw HF + MP2 energy surface) is noticeably worse. From a quantitative point of view, the deviation σ of the CC calculations from the experimental diffraction peak areas has been calculated using the formula

$$\sigma = \frac{1}{N}\sqrt{\sum_{n,m} |I^{CC}_{n,m} - I^{exp}_{n,m}|^2} \times 100, \qquad (12)$$

for each diffraction pattern, where N is the total number of experimentally observed diffraction channels, and $I^{CC}_{n,m}$ and $I^{exp}_{n,m}$ are the close-coupling and experimental peak areas for each (n, m) channel, respectively. Eqn (12) gives an overall error estimation for each diffraction pattern. In this type of analysis, this quantity is much more convenient than using a relative error for each diffraction intensity since it provides an estimate of the overall quality of the global fitting. As it can be seen from Table 2, the upscaled potential provides a substantially better description of diffraction than the bare MP2-fitted one. This result supports the conclusion that at the HF + MP2 level of theory the attractive component of the He–surface

Table 2 The values of the deviations σ of the CC calculations from the experimental diffraction peak areas for the General ($m = 2$) and upscaled attractive component potentials

	σ/%	
	Scaling factor	
Incident energy/meV	1.0	1.65
26.62	12.2	1.4
33.30	11.8	2.7
40.02	24.7	2.3
48.96	29.6	4.9
50.20	21.1	3.4
60.47	37.7	14.0

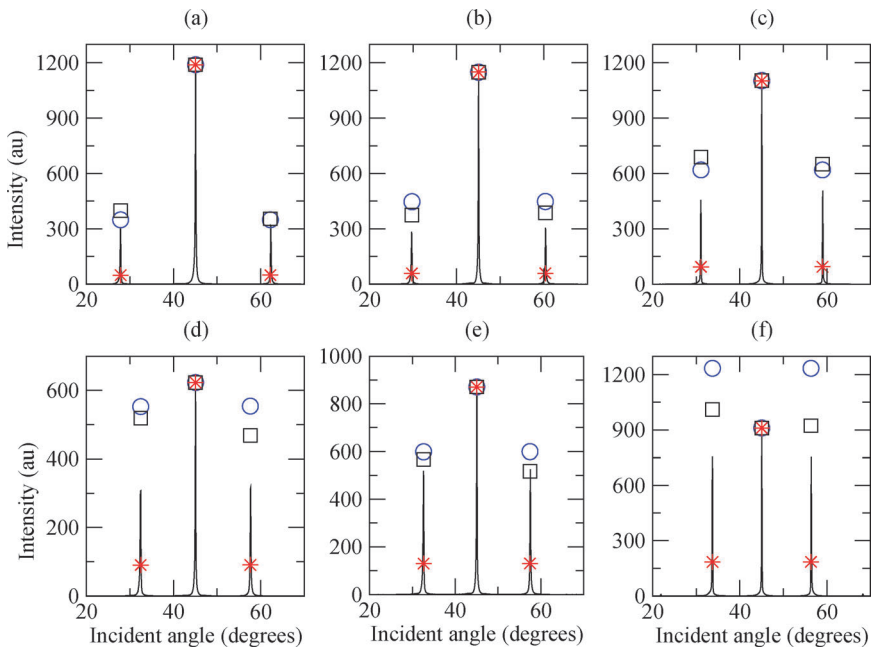

Fig. 4 Comparison of the CC intensities for case 1 (red stars) and case 2 (blue circles) with the experimental spectra (black lines) and the peak areas (black squares). Diffraction peaks are given in counts s^{-1}; peak areas and CC intensities have been normalized in a way that the specular (central) peak appears at the maximum of the experimental peak. The considered incident energies are the following: (a) $E_i = 26.62$ meV, (b) $E_i = 33.30$ meV, (c) $E_i = 40.02$ meV, (d) $E_i = 48.96$ meV, (e) $E_i = 50.20$ meV and (f) $E_i = 60.47$ meV.

interaction, although described in a qualitatively correct way, is substantially underestimated. More specifically, it manifests in underestimation of the long-range dispersion and the depth of the minimum as well as overestimation of the repulsiveness in the short range. Increasing the attractive interaction in an *ad hoc* manner corrects for all the three mentioned deficiences including the short-range part, important for the high-energy diffraction. The potential surface obtained within such a treatment allows for considerably better agreement with both the observed binding energy and diffraction intensities. The significant changes in the diffraction peaks at high incident energies is explained by the detectable influence of the upscaling on the overall interaction at short-range as can be seen in Fig. 3.

The new method is an alternative to the commonly used Eikonal approximation or Corrugated Morse potential[12,13] with the advantage of obtaining very accurate He–surface interaction potentials that are independent of the incident energy. The eikonal approximation, which uses a hard corrugated wall, has been unsucessfully applied to study strongly corrugated systems such as MgO[7] obtaining agreement in the order of magnitude of the diffraction intensities but not the required precision. This approximation is expected to overestimate the intensity when comparing to a more realistic corrugated well potential with the correct $1/z^3$ behavior of the long-range Van der Waals attraction.[44] In the case of slightly more refined methods such as the Corrugated Morse potential, there is still the problem of the dependency of the corrugation function on the incident energy and the lack of unicity, as different fitted parameters can be able to present a good agreement with the experimental data. In conclusion, the good agreement obtained between the CC results and the experimental data shows that in order to obtain an accurate description of the He–MgO diffraction process a detailed study of both the short and long range interaction is required.

IV. Conclusions

An efficient model describing the He-atom scattering process has been presented. The He–surface interaction potential has been calculated from first principles by exploiting second-order Rayleigh–Schrödinger perturbation theory in the Møller–Plesset partitioning and fitted by using a variety of pairwise interaction potentials. Based on the fitted analytical form, the intensity of the He-diffraction peaks has been calculated using the close-coupling method. When the attractive component of the potential is enhanced to allow for the underestimate of the interaction implicit in the MP2 approach good agreement between the computed and observed binding energy and diffraction intensities for the He–MgO(100) system is achieved.

As the surface interaction is dominated by the He–O potential, in the future we plan to investigate if this potential form is transferable to a wide variety of oxide surfaces and a quantitative analysis of He-atom experiments can be achieved. A further generalization of the described technique to fully first-principle determination of the interaction potentials will be presented in an upcoming contribution.

Appendix A: Appendix

The Lennard-Jones potential expressed in terms of pair interaction between helium and oxygen and between helium and magnesium takes the form:

$$V(\mathbf{r}_{He}) = \sum_i \varepsilon_{HeO}\left[\left(\frac{r_{HeO}}{|\mathbf{r}_{He}-\mathbf{r}_{O_i}|}\right)^{12} - 2\left(\frac{r_{HeO}}{|\mathbf{r}_{He}-\mathbf{r}_{O_i}|}\right)^{6}\right] + \sum_j \varepsilon_{HeMg}\left[\left(\frac{r_{HeMg}}{|\mathbf{r}_{He}-\mathbf{r}_{Mg_j}|}\right)^{12} - 2\left(\frac{r_{HeMg}}{|\mathbf{r}_{He}-\mathbf{r}_{Mg_j}|}\right)^{6}\right] \quad (A1)$$

where ε_{HeO} and ε_{HeMg} are the well depths and r_{HeO} and r_{HeMg} are the equilibrium distances between He and O and He and Mg, respectively. The variables $\mathbf{r}_{He}$, $\mathbf{r}_O$ and $\mathbf{r}_{Mg}$ represent the positions of the He, O and Mg, respectively.

In the same way the Morse potential when extending to the interaction between He and MgO surface takes the form

$$V(\mathbf{r}_{He}) = \sum_i D_{HeO}\{[1-\exp^{-a_{HeO}(|\mathbf{r}_{He}-\mathbf{r}_{O_i}|-r_{HeO})}]^2 - 1\} + \sum_j D_{HeMg}\{[1-\exp^{-a_{HeMg}(|\mathbf{r}_{He}-\mathbf{r}_{Mg_j}|-r_{HeMg})}]^2 - 1\} \quad (A2)$$

where D_{HeO} and D_{HeMg} are the well depths and a_{HeO} and a_{HeMg} the stiffness parameters of the He–O and He–Mg interactions, respectively. The Buckingham and the General potential have the same form when is expressed in terms of pair interaction between He and O, it follows:

$$V(\mathbf{r}_{He}) = \sum_i \left[A_{HeO}\exp^{\left(-\frac{|\mathbf{r}_{He}-\mathbf{r}_{O_i}|}{\rho_{HeO}}\right)}\left(\frac{1}{|\mathbf{r}_{He}-\mathbf{r}_{O_i}|}\right)^m - C_{HeO}\left(\frac{1}{|\mathbf{r}_{He}-\mathbf{r}_{O_i}|}\right)^n\right] + \sum_j \left[A_{HeMg}\exp^{\left(-\frac{|\mathbf{r}_{He}-\mathbf{r}_{Mg_j}|}{\rho_{HeMg}}\right)}\left(\frac{1}{|\mathbf{r}_{He}-\mathbf{r}_{Mg_j}|}\right)^m - C_{HeMg}\left(\frac{1}{|\mathbf{r}_{He}-\mathbf{r}_{Mg_j}|}\right)^n\right] \quad (A3)$$

where A_{HeO} and A_{HeMg} are the repulsive coefficients and C_{HeO} and C_{HeMg} the attractive ones of the He–O and He–Mg interactions, respectively. It corresponds to the Buckingham potential with $m = 0$, to the General ($m = 1$) and the General ($m = 2$). In all the case the value of n in the attactive part is 6.

Acknowledgements

RMC thanks Royal Society for Newton International Fellowship. The authors are grateful to Dr Franziska Traeger for providing the experimental results, Dr Angel Sanz-Ortiz for useful discussions, Prof. Pablo Villareal for the bound states program and Prof. Salvador Miret-Artes for the close-coupling

program. In addition, this work made use of the facilities of Imperial College HPC and—*via* our membership of the UK's HPC Materials Chemistry Consortium funded by EPSRC (EP/F067496)—of HECToR, the UK's national high-performance computing service, which is provided by UoE HPCx Ltd at the University of Edinburgh, Cray Inc and NAG Ltd, and funded by the Office of Science and Technology through EPSRC's High End Computing Programme.

References

1 F. Traeger, *ChemPhysChem*, 2006, **7**, 1006.
2 V. E. Henrich and P. A. Cox, *The Surface Science of Metal Oxides*, Cambridge University Press, Cambridge, 1996.
3 B. Johnson and R. J. Hinde, *J. Phys. Chem. A*, 2011, **115**, 7112.
4 H.-J. Freund, H. Kuhlenbeck and V. Staemmler, *Rep. Prog. Phys.*, 1996, **59**, 283.
5 G. Brusdeylins, R. B. Doak, J. G. Skofronick and J. P. Toennies, *Surf. Sci.*, 1983, **128**, 191.
6 M. Mahgerefteh, D. R. Jung and D. R. Frankl, *Phys. Rev. B: Condens. Matter Mater. Phys.*, 1989, **39**, 3900.
7 D. Jung, M. Mahgerefteh and D. R. Frankl, *Phys. Rev. B: Condens. Matter Mater. Phys.*, 1989, **39**, 11164.
8 P. Cantini and E. Cevasco, *Surf. Sci.*, 1984, **148**, 37.
9 E. Hulpke, *Helium Atom Scattering from Surfaces*, Springer Series in Surface Science, Springer, Berlin, 1992, vol. 27.
10 I. Estermann and O. Stern, *Z. Phys.*, 1930, **61**, 95.
11 G. Brusdeylins, R. B. Doak and J. P. Toennies, *Phys. Rev. Lett.*, 1981, **46**, 437.
12 R. Martinez-Casado, B. Meyer, S. Miret-Artes, F. Traeger and C. Woell, *J. Phys.: Condens. Matter*, 2007, **19**, 305006.
13 R. Martinez-Casado, B. Meyer, S. Miret-Artes, F. Traeger and C. Woell, *J. Phys.: Condens. Matter*, 2010, **22**, 304011.
14 R. Martinez-Casado, G. Mallia, D. Usvyat, L. Maschio, S. Casassa, M. Schütz and N. M. Harrison, *J. Chem. Phys.*, 2011, **134**, 014706.
15 C. Pisani, L. Maschio, S. Casassa, M. Halo, M. Schütz and D. Usvyat, *J. Comput. Chem.*, 2008, **29**, 2113.
16 M. Schütz, D. Usvyat, M. Lorenz, C. Pisani, L. Maschio, S. Casassa and M. Halo, in *Accurate Condensed-Phase Quantum Chemistry*, ed. F. R. Manby, CRC Press, Taylor and Francis, NY, 2010, pp. 29–55.
17 A. Sanz and S. Miret-Artés, *Phys. Rep.*, 2006, **451**, 37.
18 M. Hernández, O. Roncero, S. Miret-Artés, P. Villarreal and G. Delgado-Barrio, *J. Chem. Phys.*, 1989, **90**, 3823.
19 S. Miret-Artés, J. Toennies and G. Witte, *Phys. Rev. B: Condens. Matter Mater. Phys.*, 1996, **54**, 5881.
20 R. Guantes, A. S. Sanz, J. Margalef-Roig and S. Miret-Artés, *Surf. Sci. Rep.*, 2004, **53**, 199.
21 R. Blachnik, J. Chu, R. R. Galazka, J. Geurts, J. Gutowski, B. Honerlage, D. Hofmann, J. Kossut, R. Levy, P. Michler, V. Neukirch, D. Strauch, T. Story and A. Waag, *II–VI and I–VII Compounds; Semimagnetic Compounds, vol. 41B of Landolt-Brnstein—Group III Condensed Matter*, Springer Verlag, 1988.
22 J. Scaranto, G. Mallia and N. Harrison, *Comput. Mater. Sci.*, 2011, **50**, 2080.
23 R. Dovesi, V. R. Saunders, C. Roetti, R. Orlando, C. M. Zicovich-Wilson, F. Pascale, B. Civalleri, K. Doll, N. M. Harrison and I. J. Bush, *et al.*, , *CRYSTAL09 User's Manual*, Università di Torino, Torino, 2010.
24 R. Dovesi, R. Orlando, B. Civalleri, C. Roetti, V. R. Saunders and C. M. Zicovich-Wilson, *Z. Kristallogr.*, 2005, **220**, 571.
25 C. Wolken, *J. Chem. Phys.*, 1973, **3047**, 58.
26 L. Fox, *The numerical solution of two-point boundary value problems in ordinary differential equations*, Oxford University Press, London, 1957.
27 J. L. Beeby, *J. Phys. C: Solid State Phys.*, 1971, **4**.
28 https://projects.ivec.org/gulp/.
29 J. Cooley, *Math. Comput.*, 1961, **15**, 363.
30 M. Karini and G. Vidali, *Phys. Rev. B: Condens. Matter Mater. Phys.*, 1989, **39**, 3854.
31 G. Benedek, G. Brusdeylins, V. Senz, J. G. Skofronick, J. P. Toennies, F. Traeger and R. Vollmer, *Phys. Rev. B: Condens. Matter Mater. Phys.*, 2001, **64**, 125421.
32 J. Cui, D. Jung and D. Frankl, *Phys. Rev. B: Condens. Matter Mater. Phys.*, 1990, **42**, 9701.
33 D. Jung, J. Cui and D. Frankl, *J. Vac. Sci. Technol., A*, 1991, **9**, 1589.
34 G. Vidali, G. Ihm, H.-Y. Kim and M. Cole, *Surf. Sci. Rep.*, 1991, **12**, 135.
35 C. Cramer, *Essentials of Computational Chemistry*, Wiley, 2004.
36 F. Jensen, *Introduction to Computational Chemistry*, Wiley, 2007.
37 S. Tosoni and J. Sauer, *Phys. Chem. Chem. Phys.*, 2010, **12**, 14330.
38 A. Heßelmann, *J. Chem. Phys.*, 2008, **128**, 144112.
39 K. H. Rieder, *Surf. Sci.*, 1982, **118**, 57.
40 E. Zaremba and W. Kohn, *Phys. Rev. B: Condens. Matter Mater. Phys.*, 1976, **13**, 2270.
41 H. Hoinkes, *Rev. Mod. Phys.*, 1980, **52**, 933.
42 A. T. Yinnon, E. Kolodney, A. Amirav and R. B. Gerber, *Chem. Phys. Lett.*, 1986, **123**, 268.
43 *Magnetic Oxides and Related Compounds, Vol. V of Landolt-Börnstein-Group III Condensed Matter*, Springer Verlag, 1988.
44 J. Manson and K.-H. Rieder, *Phys. Rev. B: Condens. Matter Mater. Phys.*, 2000, **62**, 13142.